AFRL-VA-WP-TP-2006-344

INTEGRATED FLIGHT CONTROL AND FLOW CONTROL USING SYNTHETIC JET ARRAYS (POSTPRINT)

Yong Liu, Marcus Ciuryla, Miki Amitay, Chiman Kwan,
James H. Myatt, Xiaodong Zhang, Zhubing Ren, and John P. Casey

AUGUST 2006

THIS IS A SMALL BUSINESS INNOVATION RESEARCH (SBIR) PHASE I DOCUMENT.

Approved for public release; distribution is unlimited.

STINFO COPY

AIR VEHICLES DIRECTORATE
AIR FORCE MATERIEL COMMAND
AIR FORCE RESEARCH LABORATORY
WRIGHT-PATTERSON AIR FORCE BASE, OH 45433-7542

NOTICE AND SIGNATURE PAGE

AFRL-VA-WP-TP-2006-344 HAS BEEN REVIEWED AND IS APPROVED FOR PUBLICATION IN ACCORDANCE WITH ASSIGNED DISTRIBUTION STATEMENT.

*//Signature//

JAMES H. MYATT, Ph.D.
Senior Aerospace Engineer
Control Design and Analysis Branch
Air Vehicles Directorate

//Signature//

DEBORAH S. GRISMER, Ph.D.
Chief
Control Design and Analysis Branch
Air Vehicles Directorate

//Signature//

JEFFREY C. TROMP, Ph.D.
Senior Technical Advisor
Control Sciences Division
Air Vehicles Directorate

This report is published in the interest of scientific and technical information exchange, and its publication does not constitute the Government's approval or disapproval of its ideas or findings.

*Disseminated copies will show "//Signature//" stamped or typed above the signature blocks.

REPORT DOCUMENTATION PAGE

Form Approved
OMB No. 0704-0188

1. REPORT DATE *(DD-MM-YY)*	2. REPORT TYPE	3. DATES COVERED *(From - To)*
August 2006	Conference Paper Postprint	04/29/2005 – 01/29/2006

4. TITLE AND SUBTITLE
INTEGRATED FLIGHT CONTROL AND FLOW CONTROL USING SYNTHETIC JET ARRAYS (POSTPRINT)

5a. CONTRACT NUMBER
FA8650-05-M-3539

5b. GRANT NUMBER

5c. PROGRAM ELEMENT NUMBER
0605502

6. AUTHOR(S)
Yong Liu (Ohio University)
Marcus Ciuryla and Miki Amitay (Rensselaer Polytechnic Institute)
Chiman Kwan, Xiaodong Zhang, and Zhubing Ren (Intelligent Automation, Inc.)
James H. Myatt and John P. Casey (AFRL/VACA)

5d. PROJECT NUMBER
A08W

5e. TASK NUMBER

5f. WORK UNIT NUMBER
0B

7. PERFORMING ORGANIZATION NAME(S) AND ADDRESS(ES)

Ohio University
329 Stocker Center
Athens, OH 45701

Intelligent Automation, Inc.
15400 Calhoun Dr., Suite 400
Rockville, MD 20855

Rensselaer Polytechnic Institute
Jonsson Engineering Center
Rm 5038
110 8th Street
Troy, NY 12180

Control Design and Analysis Branch (AFRL/VACA)
Control Sciences Division
Air Vehicles Directorate
Air Force Materiel Command, Air Force Research Laboratory
Wright-Patterson Air Force Base, OH 45433-7542

8. PERFORMING ORGANIZATION REPORT NUMBER

9. SPONSORING/MONITORING AGENCY NAME(S) AND ADDRESS(ES)
Air Vehicles Directorate
Air Force Research Laboratory
Air Force Materiel Command
Wright-Patterson Air Force Base, OH 45433-7542

10. SPONSORING/MONITORING AGENCY ACRONYM(S)
AFRL-VA-WP

11. SPONSORING/MONITORING AGENCY REPORT NUMBER(S)
AFRL-VA-WP-TP-2006-344

12. DISTRIBUTION/AVAILABILITY STATEMENT
Approved for public release; distribution is unlimited.

13. SUPPLEMENTARY NOTES
This is a Small Business Innovation Research (SBIR) Phase I document.

Conference paper published in the Proceedings of the 2006 AIAA Guidance, Navigation, and Control Conference and Exhibit, published by AIAA. PAO Case Number: AFRL/WS 06-1793 (cleared July 20, 2006). Paper contains color.

14. ABSTRACT

This document was developed under a SBIR contract. In this paper, a novel integrated flight control and flow control system using synthetic jet arrays is presented. In the proposed system, a novel active flow control actuator, synthetic-jets-instrumented-wingtips were designed to enhance or replace traditional roll control of a specified airplane. Wind tunnel experiments were conducted to obtain the dynamic model of the synthetic-jets-instrumented-wing-tips. A closed-loop active flow control system was developed to reattach the flow at high angle of attacks. A high fidelity dynamic model for the airplane with the designed synthetic-jets-instrumented-wing-tips was developed based on wind tunnel experiments. A nonlinear integrated flight control and flow control system was developed and tested in simulations. Simulation results showed that the synthetic-jets-instrumented-wing-tips, in conjunction with the elevator and rudder, can effectively control the Cessna's attitude.

15. SUBJECT TERMS SBIR document, flow control, nonlinear control, synthetic jets

16. SECURITY CLASSIFICATION OF:			17. LIMITATION OF ABSTRACT:	18. NUMBER OF PAGES	19a. NAME OF RESPONSIBLE PERSON (Monitor)
a. REPORT	b. ABSTRACT	c. THIS PAGE			James H. Myatt
Unclassified	Unclassified	Unclassified	SAR	26	19b. TELEPHONE NUMBER *(Include Area Code)* N/A

Standard Form 298 (Rev. 8-98)
Prescribed by ANSI Std. Z39-18

AIAA Guidance, Navigation, and Control Conference and Exhibit
21 - 24 August 2006, Keystone, Colorado

AIAA 2006-6190

Integrated Flight Control and Flow Control Using Synthetic Jet Arrays

Yong Liu[*]
Ohio University, Athens, OH, 45701

Marcus Ciuryla[†], Miki Amitay[‡]
Rensselaer Polytechnic Institute, Troy, NY, 12180

Chiman Kwan[§]
Intelligent Automation Inc., Rockville, MD, 20855

James H. Myatt[**]
Air Vehicles Directorate, Air Force Research Laboratory, Wright-Patterson AFB, OH, 45433

Xiaodong Zhang[††], Zhubing Ren[‡‡]
Intelligent Automation Inc., Rockville, MD, 20855

John P. Casey[§§]
Air Vehicles Directorate, Air Force Research Laboratory, Wright-Patterson AFB, OH, 45433

In this paper, a novel integrated flight control and flow control system using synthetic jet arrays is presented. In the proposed system, a novel active flow control actuator, synthetic-jets-instrumented-wingtips were designed to enhance or replace traditional roll control of a specified airplane. Wind tunnel experiments were conducted to obtain the dynamic model of the synthetic-jets-instrumented-wing-tips. A closed-loop active flow control system was developed to reattach the flow at high angle of attacks. A high fidelity dynamic model for the airplane with the designed synthetic-jets-instrumented-wing-tips was developed based on wind tunnel experiments. A nonlinear integrated flight control and flow control system was developed and tested in simulations. Simulation results showed that the synthetic-jets-instrumented-wing-tips, in conjunction with the elevator and rudder, can effectively control the Cessna's attitude.

Nomenclature

C_A = control allocation matrix
c = mean chord of the wing
F_B = body frame

[*] Graduate Student, School of Electrical Engineering and Computer Science, Ohio University
[†] Graduate Student, Department of Mechanical Aerospace and Nuclear Engineering, Rensselaer Polytechnic Institute.
[‡] Assistant Professor, Department of Mechanical Aerospace and Nuclear Engineering, Rensselaer Polytechnic Institute.
[§] Senior Research Scientist, Intelligent Automation Inc.
[**] Senior Aerospace Engineer, Senior Member AIAA.
[††] Research Scientist, Intelligent Automation Inc.
[‡‡] Research Engineer, Intelligent Automation Inc.
[§§] 1st Lieutenant, Member AIAA.

F_E = earth frame

g = gravity acceleration rate (m/s^2)

I_x, I_y, I_z, I_{xz} = aircraft moment inertials (Kg m^2)

k_p = roll rate proportional feedback gain

k_{pI} = roll rate integral feedback gain

k_q = pitch rate proportional feedback gain

k_{qI} = pitch rate integral feedback gain

k_r = yaw rate proportional feedback gain

k_{rI} = yaw rate integral feedback gain

m = aircraft mass (Kg)

p = roll rate in F_B (rad/s)

p_c = roll rate command (rad/s)

$\tilde{p}$ = roll rate tracking error (rad/s)

$\tilde{p}_I$ = integral roll rate tracking error (rad)

q = pitch rate in F_B (rad/s)

q_c = pitch rate command (rad/s)

$\tilde{q}$ = pitch rate tracking error (rad/s)

$\tilde{q}_I$ = integral pitch rate tracking error (rad)

r = yaw rate in F_B (rad/s)

r_c = yaw rate command (rad/s)

$\tilde{r}$ = yaw rate tracking error (rad/s)

$\tilde{r}_I$ = integral yaw rate tracking error (rad)

T = synthetic-jet-instrumented wingtip time constant

T_f = time of flight over the wing tip

T_l = rolling moment (N.m)

T_{l_aero} = the baseline aerodynamic rolling moments on the wing-body that are not related to actuator control input (N. m)

T_{l_ctrl} = rolling moment generated by actuators (N.m)

T_m = pitching moment (N.m)

T_{m_aero} = the sum of the pitching moment generated by the engine thrust and the baseline aerodynamic pitching moments on the wing-body that are not related to actuator control input (N. m)

T_{m_ctrl} = pitching moment generated by actuators (N.m)

T_n = yawing moment (N.m)

T_{n_aero} = the baseline yawing aerodynamic moments on the wing-body that are not related to actuator control input (N. m)

T_{n_ctrl} = yawing moment generated by actuators (N.m)

U_∞ = wind tunnel freestream speed

u_B = x component of inertial velocity in F_B (m/s)

v_B = y component of inertial velocity in F_B (m/s)

V = input voltage to synthetic jets on the left wingtip (V)

V_a = air speed (m/s)

w_B = z component of inertial velocity in F_B (m/s)

x = x position of aircraft CoG in F_E (m)

y = y position of aircraft CoG in F_E (m)

z = z position of aircraft CoG in F_E (m)

α = angle of attack

λ = closed-loop system characteristics equation root

ν_0 = total virtual control

ν_{lc} = linear compensator generated virtual control

ν_{ad} = adaptive neural network generated virtual control

ϕ = roll angle (rad)

θ = pitch angle (rad)

ψ = heading angle (rad)

δ_A = aileron deflection (rad)

δ_E = elevator deflection (rad)

δ_R = rudder deflection (rad)

δ_{TH} = throttle position of engine 1 (rad)

δ_{SV} = synthetic jet wingtips input voltage (V)

ΔC_l =change of rolling moment coefficient

ΔC_n =change of yawing moment coefficient

I. Introduction

OPTIMAL aerodynamic performance that avoids flow separation on wing surfaces has been traditionally achieved by appropriate aerodynamic design of the airfoil section. However, when the wing design is driven by non-aerodynamic constraints (survivability, payload, etc.), aerodynamic performance is sometimes reduced. The lift of the resulting unconventional airfoil shape may be smaller than that of a conventional airfoil, and the drag may be much higher. Therefore, either active or passive flow control is necessary to maintain aerodynamic performance throughout the normal flight envelope. Although passive control devices (e.g. vortex generators) have proven, under some conditions, to be quite effective in delaying flow separation, they afford no proportional control and introduce a drag penalty when the flow does not separate (or when they are not needed). In contrast, active control enables coupling of the control input to flow instabilities that are associated with flow separation and thus may enable substantial control authority at low actuation levels. Furthermore, active actuation is largely innocuous except when activated and has the potential for delivering variable power. In previous studies, active control efforts have employed a variety of techniques including external and internal acoustic excitation [1], vibrating ribbons or flaps [2], and steady and unsteady blowing/bleed [3].

Recently, the synthetic jet has emerged as a versatile micro actuator for active flow control. The formation and evolution of synthetic jets are described in detail in the work of Smith and Glezer [4], Amitay and Glezer [5] [6] and Cannelle and Amitay [7]. The effectiveness of fluidic actuators based on synthetic jets is derived from the interaction of these jets with the embedding flow near the flow boundary that can lead to the formation of a quasi-closed recirculating flow region, resulting in a virtual modification in the shape of the surface. Past research work has focused on the use of open-loop actuation strategies to generate the required modulated input signals to jet arrays (Amitay and Glezer, [5] [6], Amitay et al., [8]-[14]), which is highly dependent on the availability of accurate and comprehensive wind tunnel-validated flow models. However, the underlying flow mechanisms and interactions of jet arrays are usually very complicated and highly nonlinear. Moreover, it is extremely difficult to accurately

model the changes in the system dynamics due to varied flight conditions, inevitable external disturbances and measurement noise, and actuator anomalies and failures. Therefore, the development of closed-loop nonlinear flow control approaches integrated with flight control, which can automatically compensate for modeling errors and adapt to changes in the aircraft dynamics, is particularly attractive to realize the full potential of synthetic jet technology.

In this paper, the study of a novel integrated flight control and flow control approach is presented. The block diagram of the proposed approach, shown in Fig. 1, has two main components. First, the degree of flow separation is controlled using synthetic jet arrays whose interaction with a cross flow can lead to a virtual modification of the aerodynamic shape of the surface, hence achieving the desired lift, drag, and moment forces acting on the airfoil. Conventional flow control actuators are usually driven at frequencies that are of the same order of the characteristic frequencies in the flow, which results in an unsteady flow field. In contrast, the synthetic jets operate at high frequencies (much higher than the characteristic frequency of the flow), therefore the interaction of these jets with the flow can lead to the formation of a *quasi-steady* closed recirculating flow region, resulting in a quasi-steady attached flow field (see Amitay and Glezer, [6]). Another important advantage of synthetic jets is that they are zero-mass-flux in nature; i.e., they are synthesized from the surrounding fluid. Thus, in contrast to conventional continuous or pulsed jets, synthetic jets transfer linear momentum to the flow without net mass injection across the flow boundary. Therefore, no plumbing is needed. In addition to the simplicity of operation, synthetic jet actuators are very compact. This makes them great candidates for MEMS applications where size and quantity are important. Finally, the synthetic jet actuator is designed such that it is driven by low power input and works at resonance, resulting in very low power consumption.

The second main component of the integrated flight control and flow control approach is a nonlinear adaptive control method that regulates the actuation signals to the jet arrays to provide the desired degree of flow reattachment. This nonlinear adaptive control scheme is based on the adaptive neural network augmented feedback linearization approach (Kim and Calise [15], Calise and Rysdyk [16], Johnson and Calise [17] and [18], and Johnson et al. [19]). A major advantage of the proposed nonlinear adaptive control scheme is its minimal dependence on an accurate model of the nonlinear system dynamics. Within the setting of feedback inversion control, the neural network (NN) is used to compensate for a wide range of modeling (inversion) errors and to reduce gain scheduling.

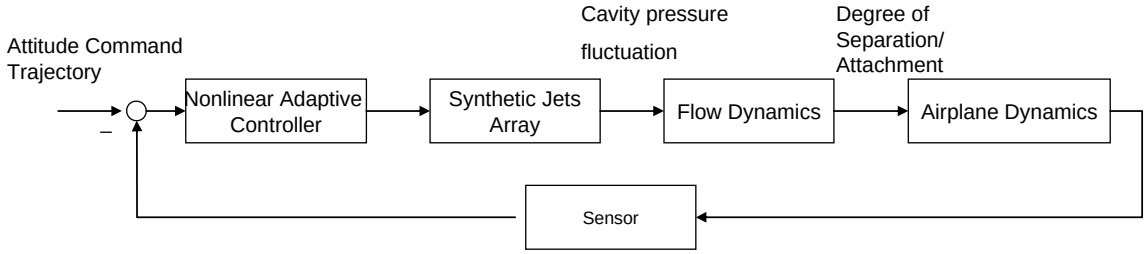

Fig. 1 A block diagram of the proposed integrated flight control and flow control scheme.

The following research objectives have been accomplished in the study of the proposed integrated flow control and flight control.

(1) A UAV with synthetic jet actuators was designed. A 1/6.65 scale Cessna 182 model was selected as the test platform for the proposed integrated flow control and flight control system. Wingtips with synthetic jets for the Cessna model were designed to enhance or replace the traditional ailerons for roll control.

(2) A Cessna 182 wind tunnel model with synthetic-jets-instrumented wingtips was designed and fabricated. The wind tunnel model of the Cessna 182 with multiple wingtip configurations was fabricated. These wingtips include aileron wingtips with different deflection angles and synthetic–jets-instrumented wingtips. The wind tunnel model was also instrumented with shear stress sensors.

(3) A large number of wind tunnel experiments were conducted to obtain the aerodynamic coefficients of the baseline Cessna using conventional ailerons and flow-controlled Cessna with synthetic–jets-instrumented wingtips.

(4) The dynamic response of the aerodynamic loads to actuation of the synthetic jet wingtips was measured in wind tunnel experiments. Using data from these experiments, a dynamic model of the synthetic-jets-instrumented wingtips was constructed.

(5) Real-time, closed-loop, active flow control for reattaching separated flow was demonstrated in the wind tunnel. As the angle of attack of the Cessna wind tunnel model was manually increased, flow separation was detected using the shear stress sensor, and the synthetic jet was automatically activated to reattach the flow.

(6) High fidelity six-degree-of-freedom (6-DOF) dynamic models of both the baseline Cessna and of the Cessna integrated with synthetic- jets-instrumented wingtips were developed.

(7) Integrated flight control and flow control for the Cessna 182 model installed with synthetic-jets-instrumented wingtips was simulated. Results showed that the synthetic-jets-instrumented wingtips in conjunction with elevator and rudder can effectively control the Cessna's attitude.

In this paper, the modeling of the dynamics of the aerodynamic response to the synthetic-jets-instrumented wingtips, the closed-loop wind tunnel experiment demonstrating flow reattachment using synthetic jets, the high fidelity simulation model of the Cessna with synthetic-jets-instrumented wingtips, and the integrated flight control and flow control design and simulation are presented. Details of other accomplishments will be presented in future publications.

II. Flow Controlled Cessna UAV Design and Cessna Wind Tunnel Model

A. Design of Cessna 182 UAV with Synthetic-Jets-Instrumented Wingtips

A scaled Cessna 182 model was purchased and built. Fig. 2 displays a photo of the Cessna 182 flying model. It has a 65 inch wingspan and is a 1/6.65 scale version of the actual aircraft. This model has dual purposes: it was used as a template for the design of the wind tunnel model as well as the flight test platform. The wingtips will be modified to hold synthetic jet modules that enhance or replace the aileron control surfaces. **Error! Reference source not found.** shows the CAD drawing of the modified wingtips instrumented with synthetic jet arrays. By introducing different actuation signals on each array, a rolling moment can be generated.

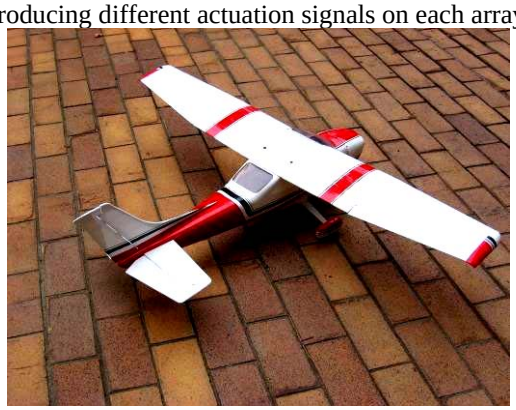

Fig. 2 Flying Model of Cessna 182.

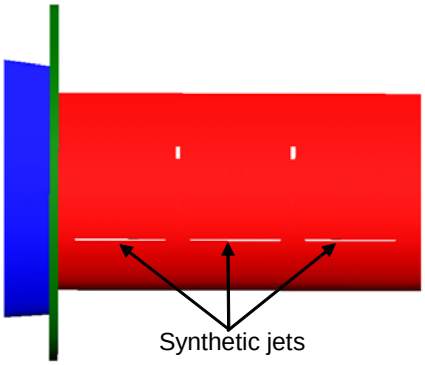

Fig. 3 Cessna synthetic-jet-instrumented wingtip

Roll control of an aircraft is typically accomplished using ailerons that are deflected in opposite directions near the tip of each wing. Significant mechanical complexity is required to control the ailerons through the use of either hydraulic lines or heavy electrical actuators and mechanical linkages. Especially if hydraulic lines are used, significant weight is added to the vehicle because ailerons are on the outboard sections of wings and the hydraulic lines must be ducted through the entire wing. Roll control using synthetic jet actuators offers potential advantages over traditional ailerons: the actuators may require less power than traditional electrical controls and the weight of the synthetic jet assemblies may be much less than hydraulic lines and pumps.

B. Cessna Wind Tunnel Model with Synthetic–Jets-Instrumented Wingtips

A wind tunnel model based on the flying Cessna 182 model has been fabricated. Measurements from the flying model airframe were used to generate a CAD model. From this computer model, a wind tunnel model was fabricated using an advanced stereolithography technique.

The wind tunnel model has an 18 in. span (1/3.6 scaled model of the 1/6.65 scaled flying model) with replaceable wingtips. The wing tips include various flap settings of the original vehicle as well as several synthetic jet configurations, as shown in Fig. 4, and are easily interchangeable. Fig. 5 shows a CAD model of the Cessna 182 main body and two symmetric wing tips instrumented with synthetic jet actuators. Fig. 6 shows the fabricated wind tunnel model with synthetic-jets–instrumented wingtips.

In the synthetic-jets-instrumented wingtips, instead of using the ailerons (for roll control), synthetic jets have been embedded within the outboard wing section. By controlling the percent of chord over which the flow is attached the lift can be differentiated from one side to the other and thus roll control can be achieved. Also shown in

Fig. 5 and Fig. 6 are fences to enforce a two dimensional flow over the wing tips. The fences are needed to model the previous work of Chatlynne, Rumigny, Amitay, and Glezer [20] on a two-dimensional (2-D) Clark-Y airfoil. In the current design the synthetic jet wing tips use the Clark-Y section similar to the previous work. The area and span of the new wingtip are identical to the original design. Wing tips without stall fences were also fabricated to determine if it is necessary to keep a 2-D flow over the controlled section of the wings.

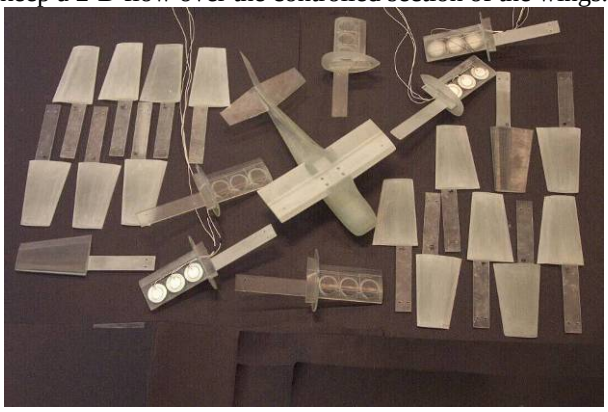

Fig. 4 Cessna wind tunnel model components (including different wing tip configurations).

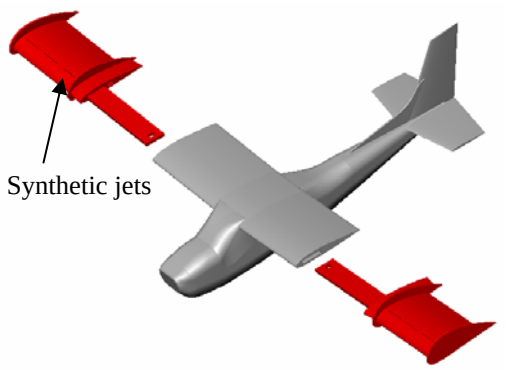

Fig. 5 Cessna wind tunnel model with flow control wing tip attachments.

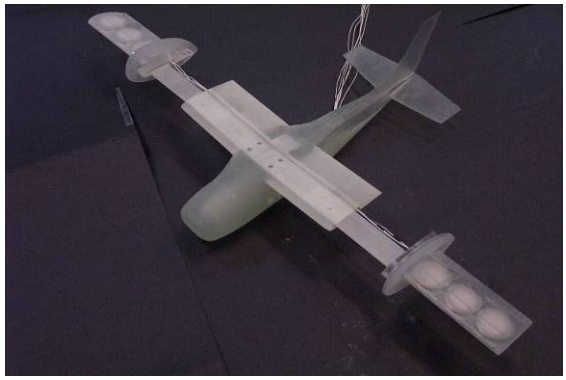

Fig. 6 Cessna wind tunnel model with synthetic–jets-instrumented wingtips.

III. Wind Tunnel Experiments for Modeling of Synthetic-Jets-Instrumented Wingtips

The analytical modeling of the aerodynamic response to the active flow control actuator is extremely difficult due to the complexity of fluid mechanics. Hence, a dynamic model of the aerodynamic response for the synthetic-jets-instrumented–wing-tips was constructed using wind tunnel data from a large number of experiments. These experiments were focused on two objectives: (1) obtaining the aerodynamic coefficients of the baseline Cessna using conventional ailerons and the flow-controlled Cessna instrumented with synthetic jets wingtips, and (2) obtaining the dynamic response of the synthetic–jets-instrumented wingtips.

The experiments were conducted in a closed-return low speed wind tunnel facility in the Department of Mechanical, Aerospace and Nuclear Engineering, Rensselaer Polytechnic Institute (RPI). Fig. 7 is an overview of the facility. The test section cross-stream has dimensions of 0.6 m x 0.6 m with a maximum velocity of 100 m/s and a turbulence level < 0.25%. Control of the wind tunnel flow speed is achieved using LabVIEW software with a closed-loop controller. The pressure and temperature are constantly monitored to correct the air speed by calculating the density. The wind tunnel is also instrumented with a 0.7 in. diameter six-component sting balance and 16 pressure transducers. Fig. 8 shows the Cessna wind tunnel model mounted on the sting balance during testing. Fig. 9 shows a zoomed-in view of the wing tip instrumented with the synthetic jets and the shear stress sensor. Table 1 contains the Cessna wind tunnel model dimension data.

Table 1 Cessna wind tunnel model data

Cessna wind tunnel model		
Mean Aerodynamic Chord	2.64	in
Span (b)	18	in
Platform area (S)	0.329514	ft^2

Fig. 7 RPI wind tunnel overview.

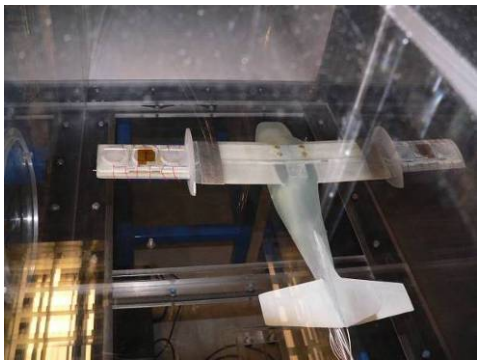

Fig. 8 Cessna 182 wind tunnel model mounted on the strut in the wind tunnel.

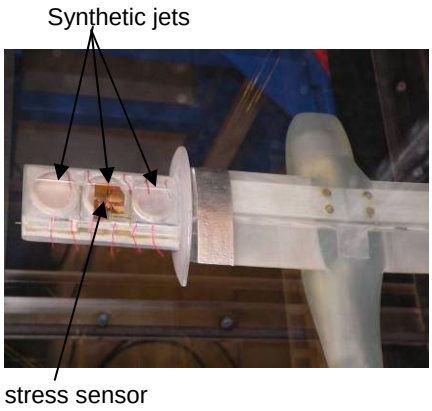

Fig. 9 Synthetic jets and shear stress sensor on Cessna 182 wind tunnel model.

A. Wind Tunnel Experimental Results for Cessna 182 with Synthetic–Jets-Instrumented Wingtips

In these experiments, the effects of the synthetic jets with different driving signals were studied. The driving signals can be characterized by input voltages, waveform and modulation frequency. In the experiments, the driving signals were set as continuous sinusoidal signals with varying input voltages. The effects of other driving signals, such as pulse width modulation, will be studied in the future.

In each experiment, three force and three moment readings from the six-component balance were obtained and transferred to forces and moments at the aerodynamic center. The aerodynamic coefficients were then calculated. The wind tunnel experiments for the Cessna using synthetic jets were categorized into two groups. The first group of experiments employed the same driving signals to the synthetic jets on both wing tips. In this configuration, experimental data showed that the lift was increased and the drag was decreased at moderate to high angles of attack. The second group of experiments employed actuation of the synthetic jets on one wing tip only; thus, roll control was achieved. The motivation for this group of experiments was to show that active flow control can be used (in selected configurations) to replace ailerons. Data were acquired for the Cessna model at different angles of attack (0 to 14 degrees), different wind tunnel speeds (50ft/s, 100ft/s and 150ft/s) and varying synthetic jets' driving voltages (0 to 3.25 V).

Fig. 10 to Fig. 13 illustrates the effects of ailerons and synthetic jets at an angle of attack of 10 degrees. Fig. 10 and Fig. 12 present the change of rolling and yawing moment coefficients when activating only synthetic jets on the left wing tip at different input voltages. Fig. 11 and Fig. 13 show the change of rolling and yawing moment coefficients due to different aileron deflection angles. From these figures, it can be seen that synthetic–jets-instrumented wing tips have several advantages over traditional ailerons. First, control authority for traditional ailerons decreases as the angle of attack increases, and at high angle of attack, control reversal may be encountered with ailerons generating reverse rolling moment. On the other hand, synthetic-jets-instrumented wingtips provide excellent roll control authority at high angle of attack (10 degrees). Another advantage of synthetic jets is that while ailerons generate adverse yawing moments (and as the angle of attack increases, adverse yawing moment increases

requiring large rudder commands), synthetic-jets-instrumented wingtips generate proverse (can't find this word) yawing moment enabling coordinated turns. Ideally, when using synthetic-jets-instrumented wingtips, the aircraft would require less yawing moment control authority for coordinated turns.

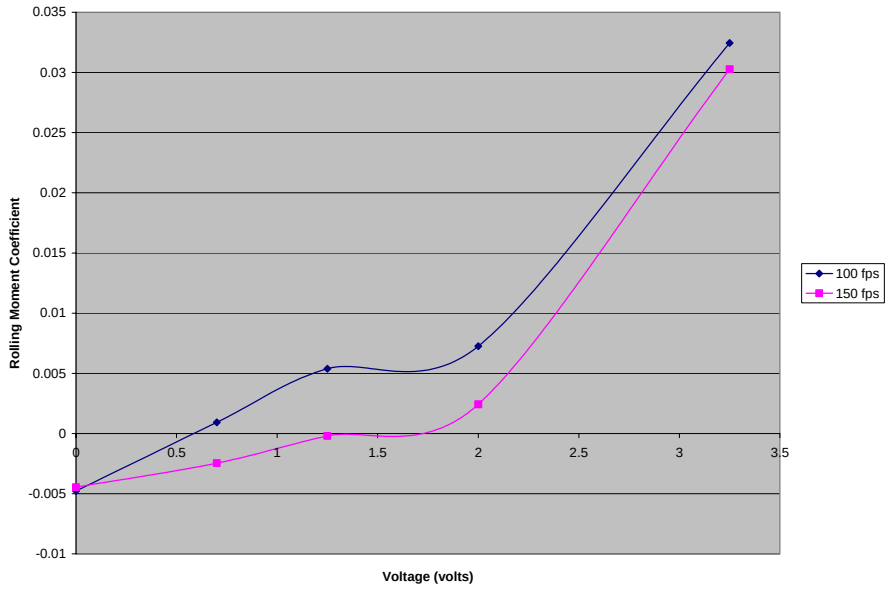

Fig. 10 Change of rolling moment coefficient ΔC_l (relative to the case with the synthetic jets inactive) with varying synthetic jets input voltages at a vehicle angle of attack of 10 degrees.

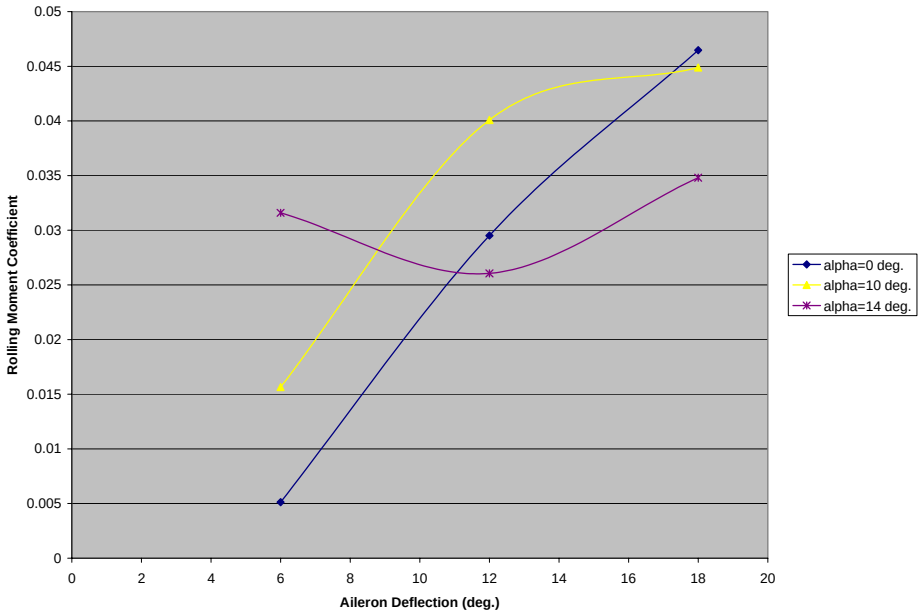

Fig. 11 Change of rolling moment coefficient ΔC_l (relative to the case with zero aileron deflection) with aileron deflection angle at a vehicle angle of attack of 10 degrees.

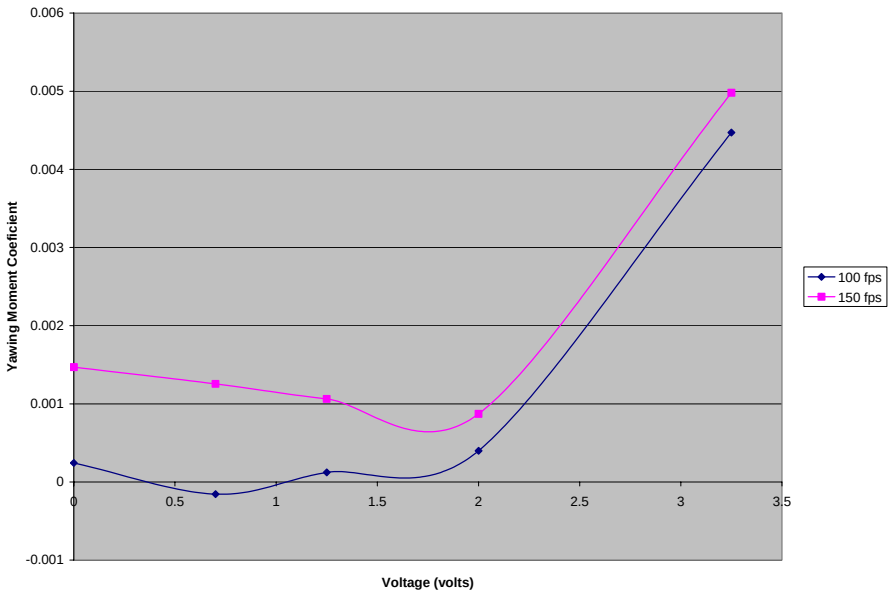

Fig. 12 Change of yawing moment coefficient ΔC_n (relative to the case with the synthetic jets inactive) with varying synthetic jets input voltages at a vehicle angle of attack of 10 degrees.

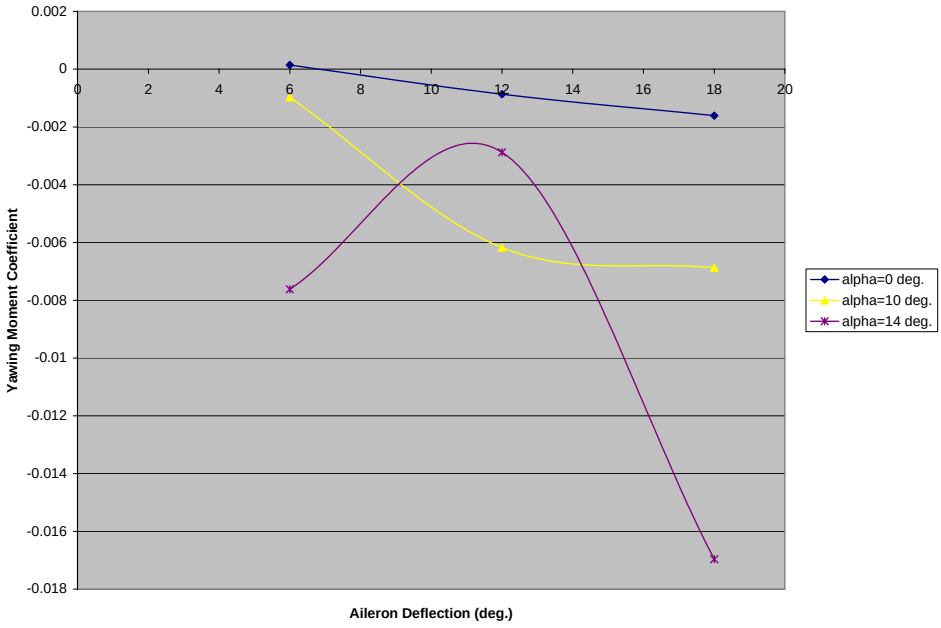

Fig. 13 Change of yawing moment coefficient ΔC_n (relative to the case with zero aileron deflection) with aileron deflection angle at a vehicle angle of attack of 10 degrees.

Because synthetic jets are only effective in separated flows, the natural question is what to do at low angles of attack where the flow is attached. In [21], significant control authority was shown on a two-dimensional airfoil at low angles of attack by using an obstruction to force the flow to separate just upstream of the synthetic jet. Wind tunnel experiments on the Cessna at low angles of attack will be conducted in the future project using wingtips with an obstruction to force separation.

Using data from Fig. 10 and Fig. 12, the increments in the rolling and yawing moment coefficients due to the synthetic jets can be approximated by the formulae in Table 2.

Table 2 Moment Coefficients for Response to Synthetic Jets.

Synthetic jets rolling moment coefficient	$\Delta C_l = f_l(V) = 0.0160V - 0.0102V^2 + 0.0027V^3$
Synthetic jets yawing moment coefficient	$\Delta C_n = f_n(V) = -0.2164\times10^{-3}V - 0.2941\times10^{-3}V^2 + 0.2349\times10^{-3}V^3$
V is the input voltage to synthetic jets on the left wing.	

B. Dynamic Model of Synthetic–Jets-Instrumented Wing Tips from Wind Tunnel Data

Wind tunnel experiments to model the dynamic responses to actuation of the synthetic–jets-instrumented wingtips were also conducted. In these experiments, the response of the shear stress sensor to a step input in voltage to the synthetic jets is used to identify the dynamic response. The signal was on for 0.5 sec and off for 0.5 sec, and the transient response of the shear stress sensors was measured by phase-locking to the onset of the input signal.

Ideally, the dynamic response is described by the aerodynamic force and moment response to the change of synthetic jets driving signals. However, a high-bandwidth force/moment balance necessary for capturing the dynamic response was not available. Instead, the shear stress sensor output was used to indicate the amount of flow separation. Since the amount of flow separation is closely related to aerodynamic forces and moments, the shear stress sensor is a suitable substitute for force and moment measurements. Thus, the dynamic response of the shear stress sensor was used to characterize the aerodynamic response to synthetic jet actuation on the wingtip.

A typical response of the shear stress sensor is illustrated in Fig. 14. The blue line in Fig. 14 is the trigger signal to apply a step input to the synthetic jets while the green line represents the shear stress sensor response. It is observed that the shear stress sensor response has components of the driving signal frequency (750 Hz) and its harmonics. Therefore, a low pass filter with cut off frequency at 400 Hz was used to filter the shear stress sensor data.

Fig. 15 shows several filtered shear stress sensor output signals. It was found that although the shear stress sensor signals shift for different combinations of wind speeds, angles of attack and different input signals, the shear stress sensor transient behaviors of all experiments are very similar. They can be described as a first order system:

$$\frac{1}{TS+1}, \text{ where } T \text{ is the time constant.}$$

From the filtered shear stress sensor data, it was estimated $T \approx 0.04 \sim 0.05$ seconds. Note that the characteristic time of the flow (the time for the freestream to travel a distance equal to one mean aerodynamic chord, $T_f = c/U_\infty$) is 0.026 sec. and 0.052 sec. for wind speeds of 100 ft/s and 50 ft/s, respectively. We can conclude that the time constant of synthetic jet wing tip can be approximated by the characteristic time of the flow.

From the experiments, the model for the aerodynamic response to the synthetic-jets wingtip actuator can be described as

$$\Delta C_l = f_l(V)\frac{1}{TS+1}$$

$$\Delta C_n = f_n(V)\frac{1}{TS+1}$$

where $f_l(V)$ and $f_n(V)$ are the coefficients model listed in Table 2.

IV. Closed-loop Active Flow Control to Reattach Flow on Cessna Wingtips

Real-time closed-loop active flow control experiments were conducted where the angle of attack of the Cessna model was manually increased from zero degree until flow separation was detected by the shear stress sensors. The shear stress sensor signal's root-mean-square (RMS) was used to detect flow separation. Once flow separation was detected, i.e. a pre-set threshold of RMS was exceeded, the synthetic jet actuators were automatically activated and the flow was reattached. During these experiments the six-component balance was also used to observe aerodynamic forces and moments during the dynamic motion of the model. Open-loop wind tunnel tests with/without synthetic jets at different angles of attack were first conducted to obtain the response of the shear stress sensor under different flow conditions.

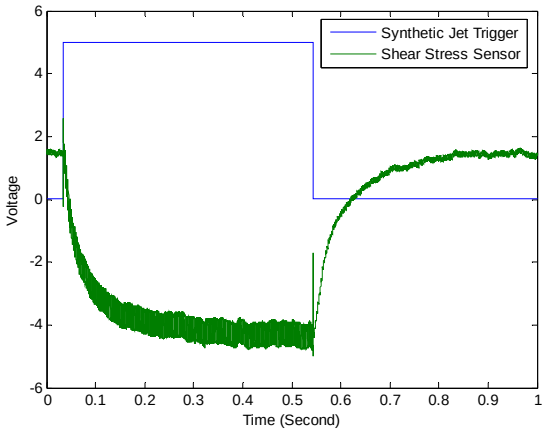

Fig. 14 Shear stress sensor response to input voltage 0.7 V to 3.25 V, wind speed = 100 ft/s, angle of attack = 12 degrees.

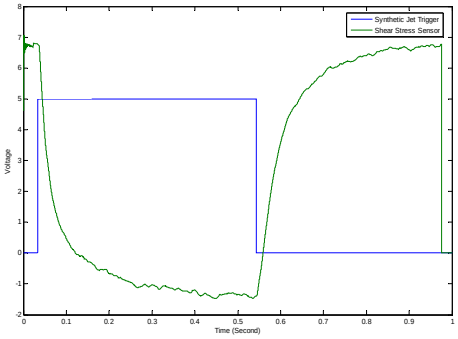

(a) Wind speed = 50 ft/s, α = 8 degrees, input voltage from 0 V to 0.7 V.

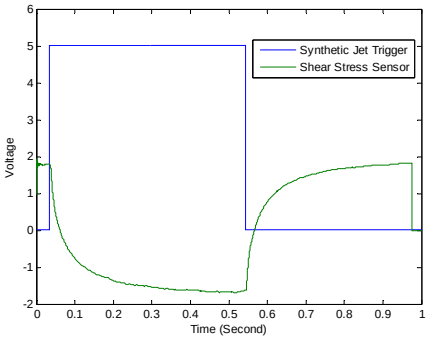

(b) Wind speed = 50 ft/s, α = 8 degrees, input voltage from 2 to 3.5 V.

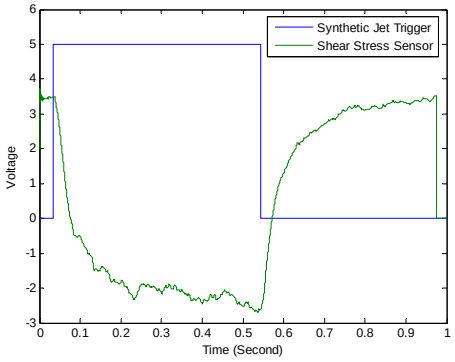

(c) Wind speed = 100 ft/s, α = 8 degrees, input voltage from 0 to 0.7 V.

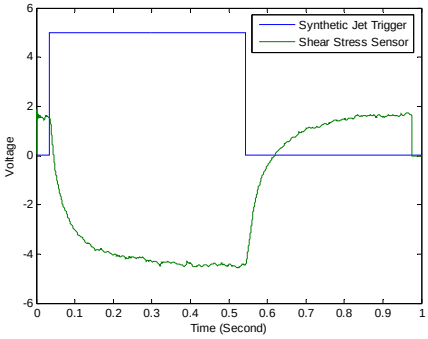

(d) Wind speed = 100 ft/s, α = 12 degrees, input voltage from 0.7 to 3.25 V

Fig. 15 Filtered shear stress sensor data.

Different flow separation thresholds were tested. Fig. 16 shows real-time closed-loop control results using a threshold of 0.5 V. Fig. 16a illustrates the shear stress sensor output signal during the increase in angle of attack from 0 degree to 8 degrees (where separation was first detected by the sensor). It can be seen that both the DC offset and the RMS of the shear stress sensor signal increased when the flow started to separate. The DC value and the RMS of shear stress sensor signal had a large abrupt increase when the flow was totally separated. The closed-loop control system detected the flow separation by comparing the signal RMS with the predefined threshold RMS. Once flow separation was detected, the closed-loop control system activated the synthetic jets on both wing tips, and

the flow was reattached. Moreover, it can be seen that the DC level of the shear stress sensor signal was reduced once the flow was reattached.

Fig. 16b shows the time trace of the six-component sting balance output of the aerodynamic forces and moments exerted on the wind tunnel model. The indicated green line is the rolling moment output. Due to the unavoidable asymmetry of the wind tunnel model caused by manufacturing imperfections, a specific side wingtip always entered stall earlier than the other side resulting in the loss of lift on this specific side and an undesired rolling moment of significant size. Such undesired rolling moments can be induced in flight at high angles of attack or due to gusts at relative low airspeed. Since one wing was already stalled, roll control using conventional aileron would have reduced authority. Thus, the undesired rolling moment could introduce large disturbance on aircraft motion and possibly cause loss of control of the aircraft. From Fig. 16(b) it can be seen that the balance sensor detected a rolling moment jump as soon as the shear stress sensor detected flow separation. After the closed-loop control activated the synthetic jets, the flow on both wing tips was reattached and the asymmetric rolling moment, generated by asymmetric wing tips, was eliminated.

In this experiment, the closed-loop control fully reattached the flow when a separation was detected. In future research, closed-loop control for commanding a specified degree of flow reattachment and thus a desired rolling moment will be explored.

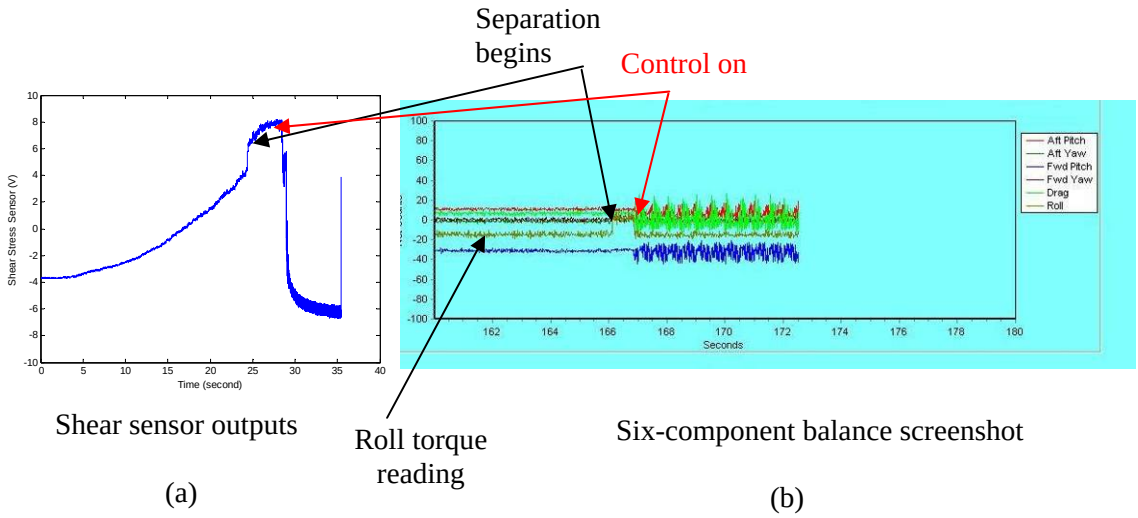

Fig. 16 Real-time closed-loop active control results with 0.5 V threshold, angle of attack increasing from 0 degree to 8 degrees.

V. Integrated Flight Control and Flow Control System for Cessna with Synthetic Jet Actuators

A. High Fidelity Simulation Model of Cessna with Flow Control Actuator

High fidelity dynamic models for both the baseline Cessna and the Cessna with synthetic–jets-instrumented wingtips were developed and implemented in Simulink. The structure of the simulation model is illustrated in Fig. 17. In this model, the wind tunnel experimental data were used to approximate the aerodynamics and the effect of the synthetic jets on the aerodynamic loads. Those aerodynamic coefficients which were not covered by wind tunnel experiments were approximated by a mathematical model of the Cessna from [22], and they will be replaced by a more realistic model when new wind tunnel experiments are conducted.

The 6-DOF Cessna dynamic model is described by the following equations, which are available in most flight dynamics text books.

Rotational Dynamics

$$\dot{\phi}=p+q\sin(\phi)\tan(\theta)+r\cos(\phi)\tan(\theta)$$

$$\dot{\theta}=q\cos(\phi)-r\sin(\phi)$$

$$\dot{\psi}=\sin(\phi)\sec(\theta)+r\cos(\phi)\sec(\theta)$$

$$\dot{p}=I_{pq}^{p}\,pq+I_{qr}^{p}\,qr+g_{l}^{p}T_{l}+g_{n}^{p}T_{n}$$

$$\dot{q}=I_{pp}^{q}\,p^{2}+I_{rr}^{q}\,r^{2}+I_{pr}^{q}\,pr+g_{m}^{q}T_{m}$$

$$\dot{r}=I_{pq}^{r}\,pq+I_{qr}^{r}\,qr+g_{l}^{r}T_{l}+g_{n}^{r}T_{n}$$

Translational Dynamics

$$\dot{u}=\tfrac{1}{m}\left(F_{x}-mgS_{\theta}\right)-qw+rv$$

$$\dot{v}=\tfrac{1}{m}\left(F_{y}+mgC_{\theta}S_{\phi}\right)-ru+pw$$

$$\dot{w}=\tfrac{1}{m}\left(F_{z}+mgC_{\theta}C_{\phi}\right)-pv+qu$$

$$\begin{bmatrix}\dot{x}\\ \dot{y}\\ \dot{z}\end{bmatrix}=\begin{bmatrix}C_{\theta}C_{\psi} & S_{\phi}S_{\theta}S_{\psi}-C_{\phi}S_{\psi} & C_{\phi}S_{\theta}C_{\psi}+S_{\phi}S_{\psi}\\ C_{\theta}S_{\psi} & S_{\phi}S_{\theta}S_{\psi}+C_{\phi}C_{\theta} & C_{\phi}S_{\theta}S_{\psi}-S_{\phi}C_{\psi}\\ -S_{\theta} & S_{\phi}C_{\theta} & C_{\phi}C_{\theta}\end{bmatrix}\begin{bmatrix}u\\ v\\ w\end{bmatrix}$$

where

$$C_{\theta}=\cos\theta, S_{\theta}=\sin\theta$$

$$C_{\phi}=\cos\phi, S_{\phi}=\sin\phi$$

$$C_{\psi}=\cos\psi, S_{\psi}=\sin\psi$$

and the rearranged moment inertias are

$$g_{l}^{p}=-\frac{I_{z}}{(I_{xz}^{2}-I_{x}I_{z})}, g_{n}^{p}=\frac{I_{xz}}{(I_{xz}^{2}-I_{x}I_{z})}, g_{m}^{q}=\frac{1}{I_{y}}, g_{l}^{r}=\frac{-I_{xz}}{(I_{xz}^{2}-I_{x}I_{z})}, g_{n}^{r}=\frac{-I_{x}}{(I_{xz}^{2}-I_{x}I_{z})}$$

$$I_{pq}^{p}=\frac{I_{xz}(I_{x}+I_{z}-I_{y})}{I_{x}I_{z}-I_{xz}^{2}}$$

$$I_{qr}^{p}=\frac{I_{z}\left(I_{y}-I_{z}\right)-I_{xz}^{2}}{I_{x}I_{z}-I_{xz}^{2}}$$

$$I_{pp}^{q}=-\frac{I_{xz}}{I_{y}}, I_{rr}^{q}=\frac{I_{xz}}{I_{y}}, I_{pr}^{q}=\frac{I_{z}-I_{x}}{I_{y}},$$

$$I_{pq}^{r}=\frac{I_{x}\left(I_{x}-I_{y}\right)+I_{xz}^{2}}{I_{x}I_{z}-I_{xz}^{2}}$$

$$I_{qr}^{r}=\frac{I_{xz}(I_{y}-I_{x}-I_{z})}{I_{x}I_{z}-I_{xz}^{2}}$$

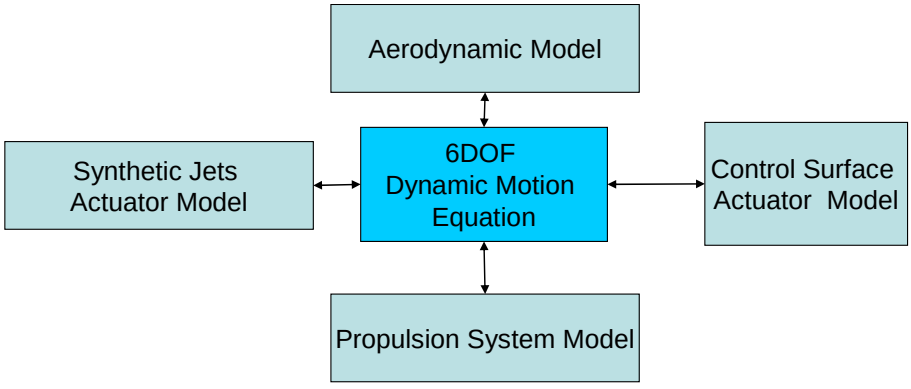

Fig. 17 High fidelity simulation model structure.

Fig. 18 shows the diagram of the Simulink simulation model for the Cessna. The actuator commands refer to engine δ_{Th}, aileron δ_A, elevator δ_E and rudder commands δ_R for the baseline Cessna. For the Cessna model with synthetic-jets- instrumented wingtips, the aileron command is replaced by input voltage δ_{SV}. δ_{SV} is defined as:

$$\delta_{SV} \in [-5,5] \text{ (V)}$$

If $\delta_{SV} > 0$, the synthetic jets on the left wing tip are activated with input voltage δ_{SV}, and the right wing tip synthetic jets are inactive. If $\delta_{SV} < 0$, the right wing tip synthetic jets are activated with an input voltage of $-\delta_{SV}$, and the left wing tip synthetic jets are inactive.

At high angles of attack, the aileron coefficients for the baseline Cessna are represented by spline functions of coefficients obtained from wind tunnel experiments. The propulsion model is described as $Thrust = \delta_{TH} mg$, where δ_{TH} is the non-unit number representing the throttle position for engine.

The dynamics of the aerodynamic responses to the synthetic jet actuators are approximated by first order systems with time constants shown in Table 3. Aileron, elevator and rudder time constants are estimated from servo data for the flying Cessna 182 model. The time constant of the aerodynamic responses for the synthetic–jets-instrumented wingtips is scaled by the factor $\sqrt{3.6}$ from the wind tunnel data. The engine time constant is estimated from experiment. In the Cessna simulation model, a wind model with six inputs is added to simulate both constant wind and turbulent conditions.

Table 3 Actuator simulation time constants.

	Time Constant (Seconds)
Aileron	0.06
Elevator	0.06
Rudder	0.06
Synthetic Jet Wingtips	0.075
Engine	0.6

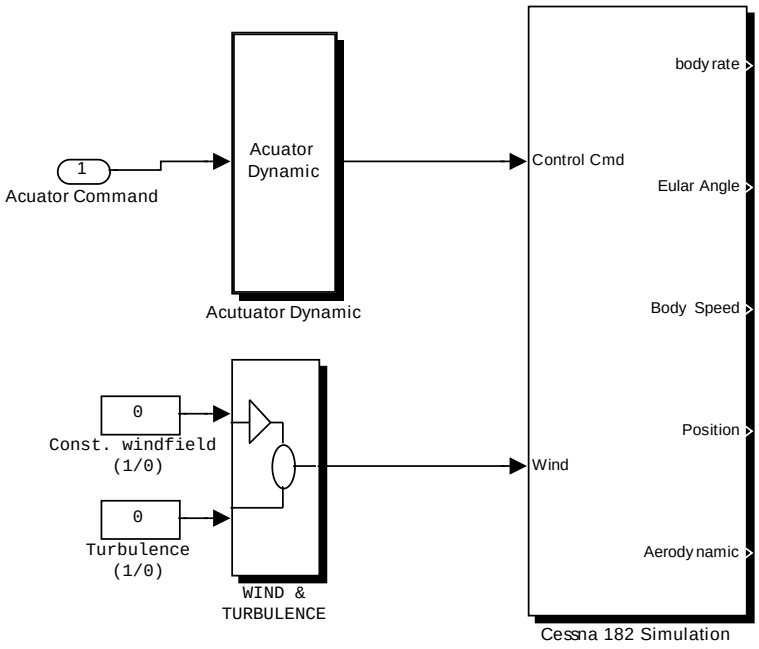

Fig. 18 Simulink simulation model diagram for the Cessna.

B. Integrated flight control and flow control system for Cessna and Simulation Results

Based on the Cessna dynamic model, an integrated flight controller (body rate controller) was designed for the Cessna instrumented with synthetic–jets-instrumented wingtips. The body rate controller is the basic block for the future autonomous flight control system. It can follow a given command by employing the synthetic-jets-instrumented wingtips, rudder and elevator.

The structure of the control system is illustrated in Fig. 19. The nominal controller is based on feedback linearization. It is augmented by an adaptive neural network controller to compensate for model uncertainty. In the current simulation model, it is found that the nominal controller itself is very robust, thus the neural network adaptive controller is not engaged. It is worth noting that although the controller is only for body rate, the Cessna full 6-DOF dynamics are simulated to evaluate controller performance.

The Cessna body rate dynamics can be rewritten as

$$\dot{p} = I_{pq}^{p}\, p\, q + I_{qr}^{p}\, q\, r + g_{l}^{p}\left(T_{l\_aero} + T_{l\_ctrl}\right) + g_{n}^{p}\left(T_{n\_aero} + T_{n\_ctrl}\right)$$

$$\dot{q} = I_{pp}^{q}\, p^{2} + I_{rr}^{q}\, r^{2} + I_{pr}^{q}\, p\, r + g_{m}^{q}\left(T_{m\_aero} + T_{m\_ctrl}\right)$$

$$\dot{r} = I_{pq}^{r}\, p\, q + I_{qr}^{r}\, q\, r + g_{l}^{r}\left(T_{l\_aero} + T_{l\_ctrl}\right) + g_{n}^{r}\left(T_{n\_aero} + T_{n\_ctrl}\right)$$

where the applied torques are divided into two parts: T_{l_aero}, T_{m_aero}, and T_{n_aero} are the sum of engine thrust generated moment and the baseline aerodynamic moments on the wing-body that are not related to actuator control input; T_{l_ctrl}, T_{m_ctrl}, and T_{n_ctrl} are actuator generated moment.

The nominal controller design can be described by the following two parts

1. *Feedback Linearization Based Control Design*

$$\begin{bmatrix} T_{l\_ctrl} \\ T_{m\_ctrl} \\ T_{n\_ctrl} \end{bmatrix} = \begin{bmatrix} g_{l}^{p} & 0 & g_{n}^{p} \\ 0 & g_{m}^{q} & 0 \\ g_{l}^{r} & 0 & g_{n}^{r} \end{bmatrix}^{-1} \begin{bmatrix} -\left(I_{pq}^{p}\, p\, q + I_{qr}^{p}\, q\, r\right) + \dot{p}_{c} - k_{p}\tilde{p} - k_{pI}\tilde{p}_{I} \\ -\left(I_{pp}^{q}\, p^{2} + I_{rr}^{q}\, r^{2} + I_{pr}^{q}\, p\, r\right) + \dot{q}_{c} - k_{p}\tilde{q} - k_{qI}\tilde{q}_{I} \\ -\left(I_{pq}^{r}\, p\, q + I_{qr}^{r}\, q\, r\right) + \dot{r}_{c} - k_{c}\tilde{r} - k_{rI}\tilde{r}_{I} \end{bmatrix} - \begin{bmatrix} T_{l\_aero} \\ T_{m\_aero} \\ T_{n\_aero} \end{bmatrix}$$

where p_c, q_c and r_c are body rate commands, $\tilde{p} = p - p_c, \tilde{q} = q - q_c, \tilde{r} = r - r_c$ are tracking errors, $\tilde{p}_I = \int_0^t \tilde{p} d\tau, \tilde{q}_I = \int_0^t \tilde{q} d\tau$, $\tilde{r}_I = \int_0^t \tilde{r} d\tau$ are integral tracking errors, k_p, k_{pI}, k_q, k_{qI}, k_r and k_{rI} are feedback gains. Therefore, the body rate closed-loop controller has the following characteristic equations

$$\begin{bmatrix} \lambda^{2} + k_{p}\lambda + k_{pI} \\ \lambda^{2} + k_{q}\lambda + k_{qI} \\ \lambda^{2} + k_{r}\lambda + k_{rI} \end{bmatrix} = \begin{bmatrix} 0 \\ 0 \\ 0 \end{bmatrix}$$

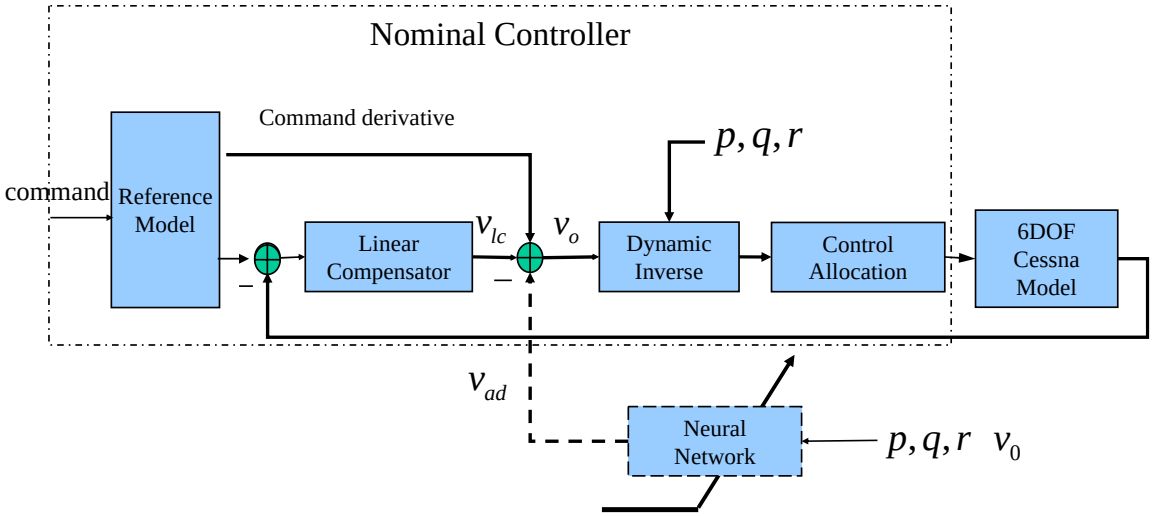

Fig. 19 Integrated flight control and flow control system structure.

2. *Controller Allocation*

From the Cessna rotation dynamic equations, we can derive

$$\begin{bmatrix} T_{l\_ctrl} \\ T_{m\_ctrl} \\ T_{n\_ctrl} \end{bmatrix} = C_A \begin{bmatrix} \delta_{SV} \\ \delta_T \\ \delta_R \end{bmatrix}$$

where C_A is the controller allocation matrix obtained from the actuator model. Thus the actuator command can be calculated as

$$\begin{bmatrix} \delta_{SV} \\ \delta_E \\ \delta_R \end{bmatrix} = C_A^{-1} \begin{bmatrix} T_{l\_ctrl} \\ T_{m\_ctrl} \\ T_{n\_ctrl} \end{bmatrix}$$

In the controller design process, the synthetic jets coefficient described in Table 2 is simplified as in Table 4, which simplifies the control reallocation design.

The controller parameters are shown in Table 5. It is worth noting that comparing the controller closed-loop bandwidth, the actuator time constant shown in Table 5 is much faster. The bandwidths of all actuators are more than 3 times larger than the desired controller closed-loop bandwidths. Thus the actuator dynamics can be ignored in the controller design process. The model error induced by simplification during the controller design process can be compensated for by the closed-loop control, which is verified by the simulation results. The Simulink simulation of integrated flight control using synthetic jets is shown in Fig. 20.

Table 4 Synthetic jets coefficient for controller design

Synthetic jets rolling moment coefficient	$\Delta C_l = 0.0098\delta_{SV}$
Synthetic jets yawing moment coefficient	$\Delta C_n = 0$

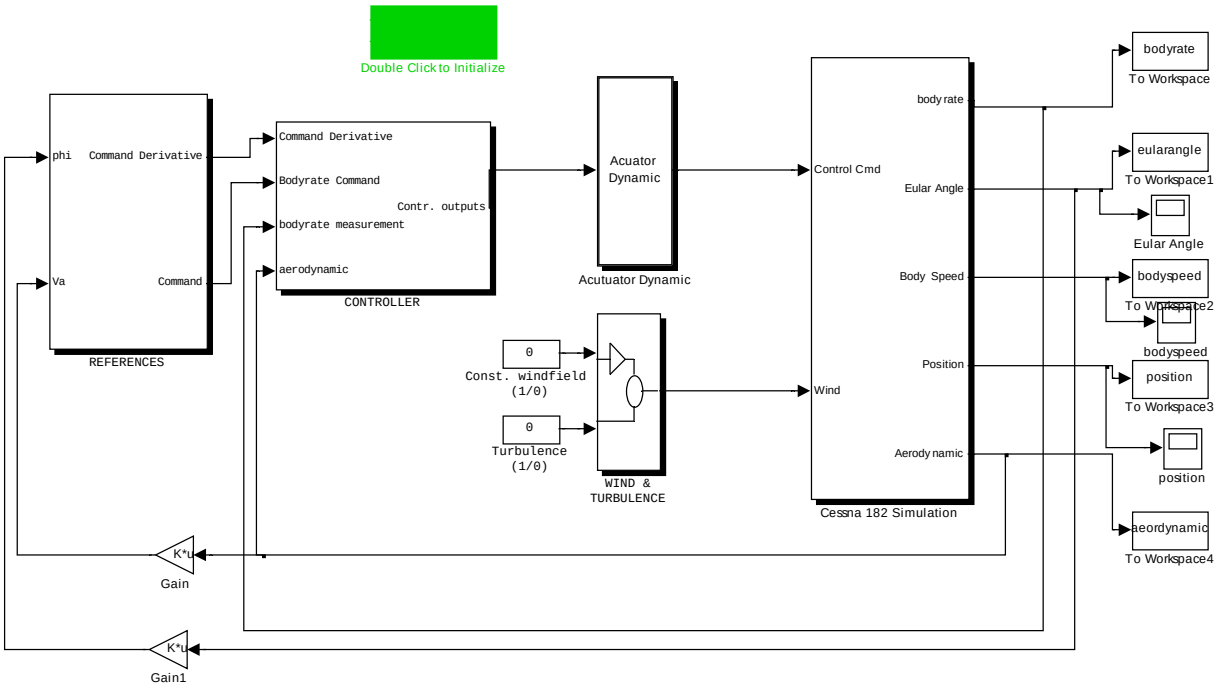

Fig. 20 Simulation of integrated flight control system using synthetic jets.

Table 5 Controller Parameters

	Command filter and controller closed-loop characteristic bandwidth	Proportional gain	Integral Gain
p channel	2	2.828	4
q channel	1	1.414	1
r channel	1	1.414	1

C. Simulation Results of Integrated Flight Control and Flow Control

In the simulation of integrated flight control and flow control, the simulation scenario is the Cessna approaching the runway for landing. The angle of attack is 6 degrees implying the local angle of attack of the synthetic-jets-instrumented wingtip is 10 degrees.

By using the trim program of the simulation model, the trim condition is

$$\delta_e = -0.2887 rad, \delta_{TH} = 0.1612, u_b = 11.6702 \text{ (m/s)}, w_b = 1.1481 \text{ (m/s)}$$

The command to the Cessna is a coordinated turn during approach given by

$$r_c = \frac{g \tan(\phi)}{V_a},$$

where V_a is the air speed.

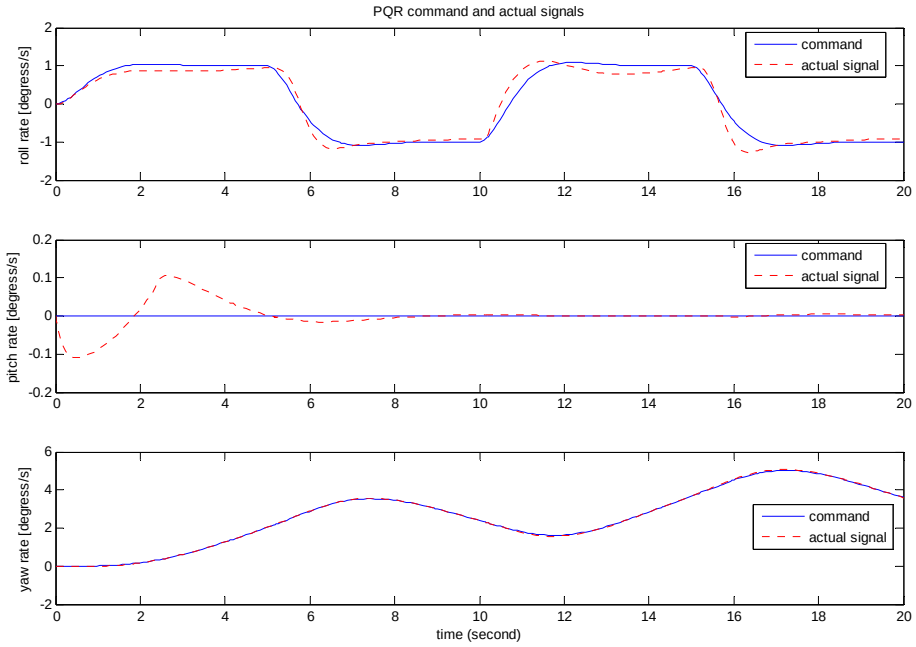
PQR command and actual signals
roll rate [degress/s]
pitch rate [degress/s]
yaw rate [degress/s]
command
actual signal
time (second)

(a)

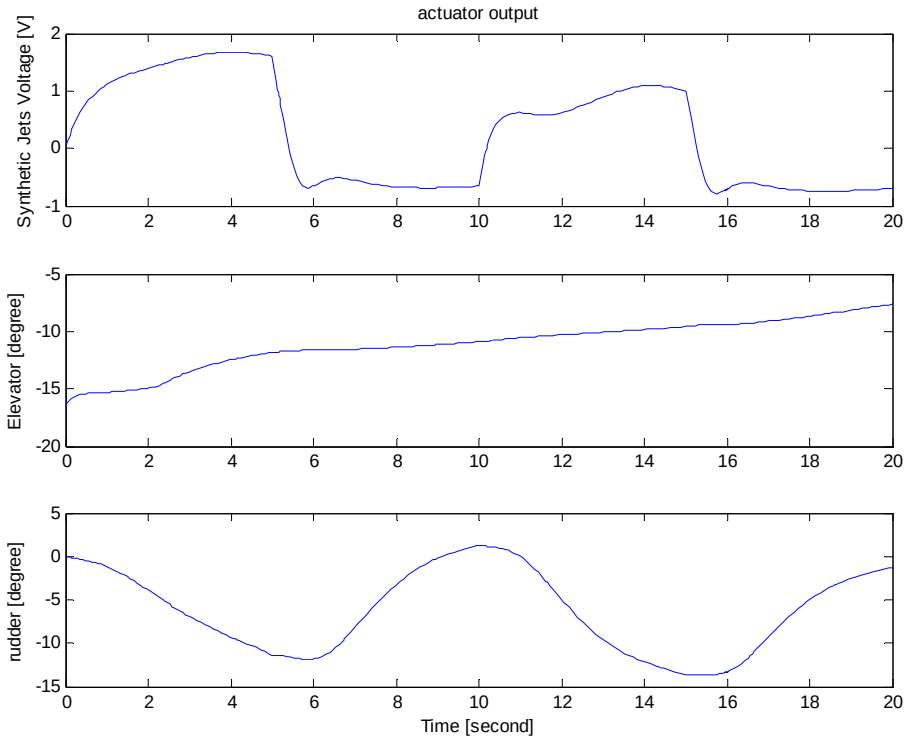
actuator output
Synthetic Jets Voltage [V]
Elevator [degree]
rudder [degree]
Time [second]

(b)

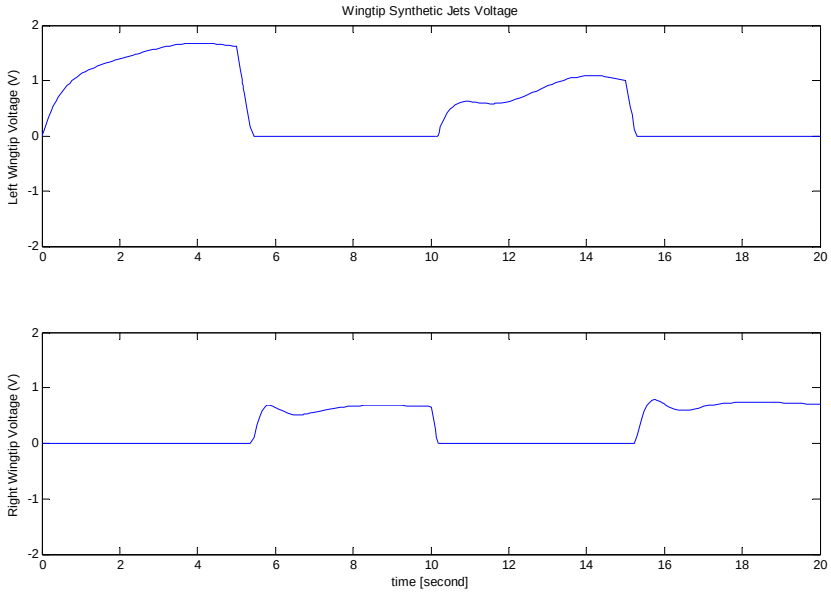

(c)

Fig. 21 Coordinated turn during approach.

Fig. 21 shows the simulation result for the coordinated turn during approach. Fig. 21a shows the body rate command and simulated Cessna response. Fig. 21b shows the actuator command to synthetic-jets-instrumented wingtip, elevator and rudder, and Fig. 21c shows the input voltage to each wingtip's synthetic jets.

From these simulation results, it can be seen that the synthetic-jets-instrumented wingtip is capable of replacing the traditional aileron and provide enough control authority for roll. It is worth noting that during the controller design, the synthetic-jets-instrumented wingtip moment coefficient due to actuation is replaced by a much simplified model relative to the real model of the effects of the synthetic jets, and that the closed-loop flight control is robust to the model error introduced by the controller design process.

VI. Conclusions and Future Work

In this paper, a novel integrated flight control and flow control approach is proposed. Some preliminary research results are presented. First, the dynamic model of synthetic-jets-instrumented wingtips was constructed from wind tunnel data. Second, a high fidelity simulation package for a scaled Cessna model with synthetic-jets-instrumented wingtips were built using wind tunnel data. Third, the closed-loop flow reattachment using synthetic jets was demonstrated in a real-time wind tunnel experiment. Fourth, integrated flight control and flow control system was designed and simulated, which clearly demonstrated that the synthetic jets can be used to control and follow a desired trajectory.

In the future, more wind tunnel experiments will be conducted to obtain the aerodynamic properties of the synthetic-jets-instrumented wingtips at low angles of attack. Wingtips instrumented with synthetic jets for the scaled flying Cessna model will be fabricated. Flight tests will be conducted with an on-board integrated flight control and flow control system.

Acknowledgment

This work is supported by the Air Force Research Laboratory, Air Vehicles Directorate, under contract FA8650-05-M-3539.

References

1. Ahuja, K. K. and Burrin, R. H., "Control of Flow Separation by Sound," AIAA Paper 1984-2298, 9th Aeroacoustics Conference, Williamsburg, VA, Oct. 1984.
2. Amitay, M. and Cannelle, F., "Evolution of Finite Span Synthetic Jets," Submitted to *Phys. of Fluids*," September 2005.
3. Neuberger, D. and Wygnanski, I., The Use of a Vibrating Ribbon to Delay Separation on Two Dimensional Airfoils, Proceedings of the Air Force Academy Workshop on Unsteady Separated Flow, Rept. TR-88-000, 1987.
4. Smith, B. L. and Glezer, A., "The formation and evolution of synthetic jets," *Physics of Fluids*, Vol. 10, No. 9, Sept. 1998, pp. 2281-2297.
5. Amitay, M. and Glezer, A., "Controlled transients of flow reattachment over stalled airfoils," *Int. Journal of Heat and Fluid Flow*, Vol. 23, Issue 5, Oct. 2002, pp. 690-699.
6. Amitay, M. and Glezer, A., "Apparatus and method for enhancement of aerodynamic performance by using pulse excitation control of synthetic jet actuators," U.S. Patent 6,412,732 B1, July 2, 2002.
7. Cannelle, F. and Amitay, M., "Synthetic Jets: Spatial Evolution and Transitory Behavior," AIAA Paper 2005-0102, 43rd AIAA Aerospace Sciences Meeting, Reno, NV, Jan. 2005.
8. Amitay, M., Horvath, M., Michaux, M., and Glezer, A., "Virtual Aerodynamic Shape Modification at Low Angles of Attack using Synthetic Jet Actuators", AIAA Paper 2001-2975, 31st AIAA Fluid Dynamics Conference, Anaheim, CA, June 2001.
9. Amitay, M., Pitt, D. and Glezer, A., "Separation Control in Duct Flows," *Journal of Aircraft*, Vol. 39, No. 4, July-Aug. 2002, pp. 616-620.
10. Amitay, M., Smith, B. L. and Glezer, A., "Aerodynamic Flow Control Using Synthetic Jet Technology," AIAA Paper 1998-0208, 36th Aerospace Sciences Meeting, Reno, NV, Jan. 1998.
11. Amitay, M., Smith, D. R., Kibens, V., Parekh, D. E. and Glezer, A., "Aerodynamic Flow Control over an Unconventional Airfoil Using Synthetic Jet Actuators", AIAA Journal 39(3), 2001, pp. 361-370.
12. Amitay, M., Washburn, A.E., Anders, S.G., Parekh, D.E. and Glezer, A., "Active Flow Control on the Stingray UAV: Transient Behavior," AIAA Paper 2003-4001, 33rd AIAA Fluid Dynamics Conference, Orlando, FL, June 2003.
13. Amitay, M., Washburn, A. E., Anders, S. G. and Parekh, D. E., "Active Flow Control on the Stingray Uninhabited Air Vehicle: Transient Behavior," *AIAA Journal*, Vol. 42, No. 11, Nov. 2004, pp. 2205-2215.
14. Allan, B.G., Juang, J-N, Raney, D.L., Seifert, A., Pack, L.G. and Brown, D.E., "Closed-loop Separation Control Using Oscillatory Flow Excitation," NASA/CR-2000-210324, NASA Langley Research Center, Hampton, VA, Aug. 2000.
15. Kim, B.S. and Calise, A. J., "Nonlinear Flight Control Using Neural Networks," *Journal of Guidance, Control, and Dynamics*, Vol. 20, No. 1, Jan.-Feb. 1997, pp. 26-33.
16. Calise, A. J. and Rysdyk, R., "Nonlinear Adaptive Flight Control Using Neural Networks," *Control Systems Magazine*, Vol. 18, Issue 6, December 1998, pp. 14-25.
17. Johnson, E. N. and Calise, A. J., "Neural Network Adaptive Control of Systems with Input Saturation," Proceedings of the 2001 American Control Conference, Vol. 5, Arlington, VA, June 2001, pp. 3527-3532.
18. Johnson, E.N. and Calise, A.J., "Pseudo-Control Hedging: A New Method for Adaptive Control," Advances in Navigation, Guidance, and Control Technology Workshop, Redstone Arsenal, AL, Nov. 2000.
19. Johnson, E.N., Calise, A.J., El-Shirbiny, H.A. and Rysdyk, R.T., "Feedback Linearization with Neural Network Augmentation Applied to X-33 Attitude Control," AIAA Guidance, Navigation, and Control Conference, Denver, CO, Aug. 2000.
20. Chatlynne, E., Rumigny, N., Amitay, M. and Glezer,A., "Virtual Aero-Shaping of a Clark-Y Airfoil Using Synthetic Jet Actuators," AIAA Paper 2001-0732, 39th Aerospace Sciences Meeting, Reno, NV, Jan. 2001.
21. Roskam, J., Airplane Flight Dynamics and Automatic Flight Controls, DAR Corporation, Lawrence, KS, 1995.